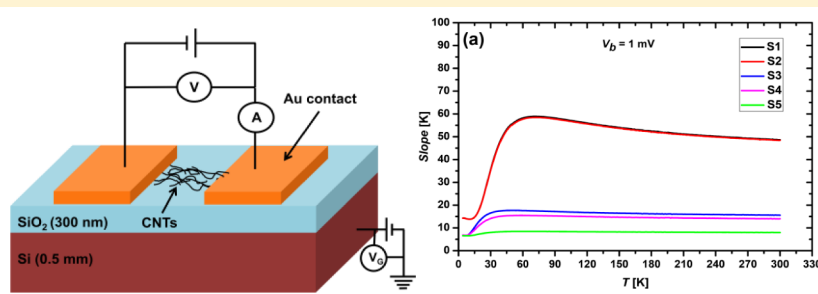# Effect of Tunnel Junctions and Coulomb Blockade on Semiconducting Property of Networks of Single-Wall Carbon Nanotubes

Mir Massoud Aghili Yajadda*

CSIRO Manufacturing Flagship, P.O. Box 218, Lindfield, NSW 2070, Australia

ABSTRACT: The optical and electrical characterization techniques were employed to demonstrate both experimentally and theoretically (parallel nonlinear resistor model) that the existence of tunnel junctions between semiconducting single-wall carbon nanotubes implies that the Coulomb blockade effect dominates their semiconducting property. Multiwall carbon nanotubes were added to a network of single-wall carbon nanotubes, and Raman spectroscopy and UV−vis−NIR spectroscopy enabled us to observe the semiconducting property of individual single-wall carbon nanotubes in a network with a high concentration of multiwall carbon nanotubes. However, the field effect measurement at 300 K on the network of single-wall carbon nanotubes and the electrical tunnel current measurements over a wide temperature range (4−300 K) at different bias voltages (0.001−10 V) on all of the networks revealed that the networks can be treated as networks of disordered metallic nanoparticles and the semiconducting property of single-wall carbon nanotubes is significantly diminished. Furthermore, we demonstrate that the electron tunneling in networks of carbon nanotubes cannot be fully described by models such as Efros−Shklovskii, Mott variable range hopping, electron cotunneling, or fluctuation-induced tunneling because of the diameter and length distributions in the networks. The effect of tunnel junctions on the performance of such networks for sensing applications and field effect transistors is discussed.

INTRODUCTION

Single-wall carbon nanotubes (SWCNTs) can be used in many applications such as field effect transistors (FETs),[1−3] nano-chromatography,[4,5] gas sensing,[6] flow sensing,[7] chemical sensing,[8] optical sensing,[9] biosensing,[10] and chemiresistors.[11] The devices that are used in such applications are commonly made of networks of SWCNTs. Therefore, understanding both the optical and the electrical properties of networks of SWCNTs is quite essential in designing such devices. The effect of tunnel junction resistance (TJR) between a SWCNT and contact electrodes on performance of the FETs has been investigated in the past.[1] In networks of SWCNTs where they are coupled via tunnel junctions, TJRs can significantly affect the conductivity of such networks.[11,12] At low bias voltages, the effect of TJRs on the electronic property of SWCNT networks has been investigated at room temperature[12] and at low temperatures.[13−17] The previous comprehensive study on mats of metallic SWCNTs indicated that electrons are strongly localized within SWCNTs at low temperatures due to defects in SWCNTs rather than tunnel junctions between SWCNTs.[18] Here, we investigate the optical and the electrical properties of

a network of SWCNTs, networks of mixed SWCNTs and multiwall CNTs (MWCNTs), and a network of MWCNTs by Raman spectroscopy, UV−vis−NIR spectroscopy, field effect measurement at 300 K and by measuring the tunnel currents over a wide temperature range (4−300 K) at different bias voltages (0.001−10 V). We show that the semiconducting property of individual SWCNTs can be observed in the network of SWCNTs and in the mixed networks by optical characterization techniques, whereas the electrical measurements show the semiconducting properties of individual SWCNTs in those networks are significantly diminished. Using the parallel nonlinear resistor model (PNRM),[19] it is shown that the tunnel junctions between CNTs play a dominant role in such networks and the Coulomb blockade effect of individual SWCNTs overshadows their semiconducting property. Unlike other theoretical models such as Efros−Shklovskii,[20] Mott variable range hopping,[20] electron cotunnel-

ing,[21] or fluctuation-induced tunneling,[22,23] which are applicable over a narrow temperature range or at the limited bias voltages, the PNRM fitted very well to the experimental data over a wide temperature range (4−300 K) at different bias voltages (0.001−10 V) and enabled us to describe the conduction mechanism in the samples comprehensively. Our investigations indicate that the semiconducting property of individual SWCNTs prevails in networks of SWCNTs and makes them suitable for the applications that only require optical measurements. In contrast, the tunnel junctions between SWCNTs can significantly change the electronic property of such networks. Therefore, the performance of devices that depends on the semiconducting property of individual SWCNTs declines significantly.

■ EXPERIMENTAL SECTION

SWCNTs (704121) and MWCNTs (755117) were purchased from Sigma-Aldrich. The diameters of SWCNTs were $d = 0.7−1.1$ nm, and the average diameter of MWCNTs was $d = 9.5$ nm. The lengths of SWCNTs were $L = 0.3−2.3$ μm, and the average length of MWCNTs was $L = 1$ μm. The transmission electron microscope image of SWCNTs can be found somewhere else.[5] To prepare the samples, sodium dodecyl sulfate (SDS) was dissolved in deionized water (0.01 wt % solution) and a mixture of SWCNTs/MWCNTs with the weight ratios of 1.0 (mg)/0.0 (mg), 0.75/0.25, 0.5/0.5, 0.25/0.75, and 0.0/1.0 was dispersed in 18 mL of SDS solution to make samples S1−S5, respectively. Then, samples were sonicated for 1 h using Sonics Vibra Cell VCX130, and a small droplet of each solution was dropped on five separate SiO_2/Si (300 nm/0.5 mm thicknesses) substrates. After samples dried on the substrate they were washed with deionized water and dried by nitrogen gas. Two square gold contact electrodes (5×5 mm^2, 100 nm thick) were deposited on the CNT networks by dc magnetron sputtering; five (approximately 0.2×0.2 mm^2) thin films of CNTs were formed between two electrodes (Figure 1). The optical
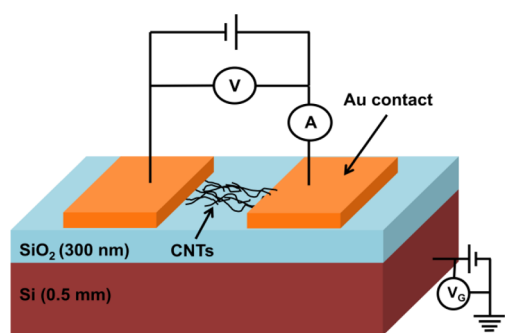

Figure 1. Schematic of the experimental setup for the electrical and the field effect measurements.

properties of samples were investigated by using Raman spectroscopy (Renishaw inVia) and UV−vis−NIR spectroscopy (Cary 5000 spectrophotometer). The electrical measurements were carried out in a physical property measurement system (Quantum Design model 6000) where the pressure was 10^{-2} Pa. The tunnel currents were measured using a picoammeter (Keithley 6485) by applying dc voltages (0.001−10 V) to the samples over the temperature range of 4−300 K. The field effect measurement on S1 was carried out at 300 K by applying dc gate voltages ($V_G = -30$ to 30 V) to the Si layer (Figure 1).

■ RESULTS AND DISCUSSION

Figure 2 shows the absorption spectra of S1−S5 at the wavelengths of $\lambda = 300−1350$ nm. Two main peaks at 660 and
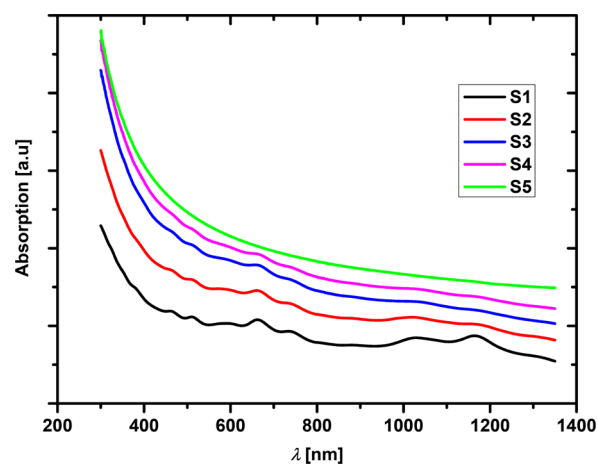

Figure 2. Absorption spectra of S1−S5. The two main peaks at 660 and 1165 nm in S1−S4 indicate the majority of s-SWCNTs have (7,6) chirality.

1165 nm can be seen for S1−S4, but the peaks significantly decrease in S4 and they completely disappear in S5 as there was no semiconducting SWCNT (s-SWCNT) in S5. These peaks are characteristics of s-SWCNTs with (7,6) chirality, which have been demonstrated previously.[24,25] In Figure 2, few weaker peaks can be observed that indicate there is a low concentration of SWCNTs with other chiralities.[24]

To further investigate the optical property of the samples, we performed Raman spectroscopy using the excitation wavelength of $\lambda = 633$ nm (Figure 3). All of the samples show a graphitic peak (G-peak) at 1592 cm^{-1} and a defective peak (D-peak) at 1330 cm^{-1}. The G-peak is much stronger than the D-peak in samples S1−S4, which indicates SWCNTs have a high quality.[17] In contrast, sample S5 has more defects in it, as D-peak is stronger than G-peak. Figure 3b depicts the radial-breathing modes (RBMs) of SWCNTs in S1−S4. There are two main peaks at 260 and 286 cm^{-1} corresponding to RBM modes of s-SWCNTs with diameters of 0.95 and 0.87 nm, respectively.[17] In sample S5, no RBM mode can be detected, as there was no SWCNT in S5.

These optical characterizations suggest the semiconducting property of individual s-SWCNTs can be observed while s-SWCNTs are coupled via tunnel junctions even in sample S4, which has a low concentration of s-SWCNTs.

In order to investigate the performance of sample S1 as a FET, a bias voltage of $V_b = 5$ V was applied to the sample while different gate voltages $V_G = -30$ to 30 V were applied to Si layer at 300 K (Figure 1). Figure 4 demonstrates the tunnel current enhancement (I_{On}/I_{Off}) as a function of gate voltage. The response of sample S1 is quite weak; the tunnel current enhancement at $V_G = -30$ V is only 1.5 and at $V_G = 30$ V is 0.6. The value of I_{On}/I_{Off} in a FET made of an individual s-SWCNT at 300 K can be as high as 10^5, which is significantly higher than I_{On}/I_{Off} of the network of SWCNTs in S1.[2] In the following we will show that the weak efficiency of S1 is mainly caused by the tunnel junctions between SWCNTs and the Coulomb blockade effect of SWCNTs.
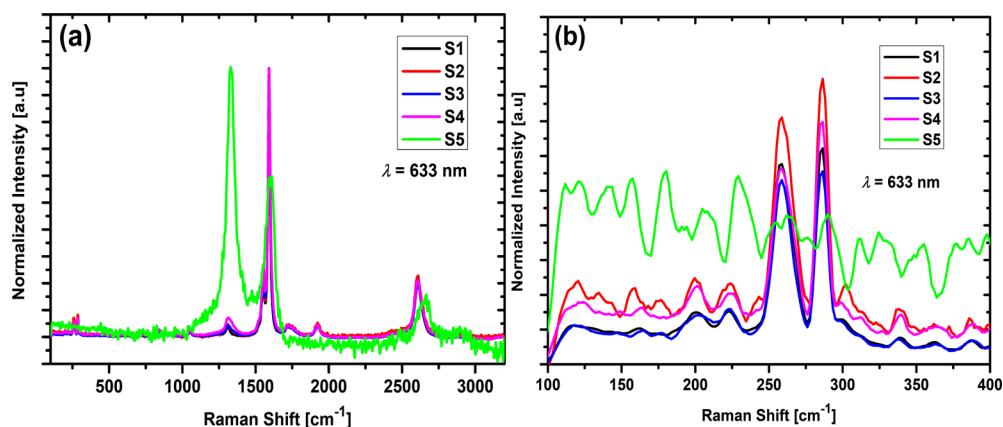
Figure 3. (a) Raman spectra of samples S1−S5 using the excitation wavelength of $\lambda = 633$ nm. (b) RBM modes of the samples. Two RBM modes are observed in S1−S4 at 260 and 286 cm^{-1}, and no RBM mode is detected in S5 because there was no SWCNT in S5.
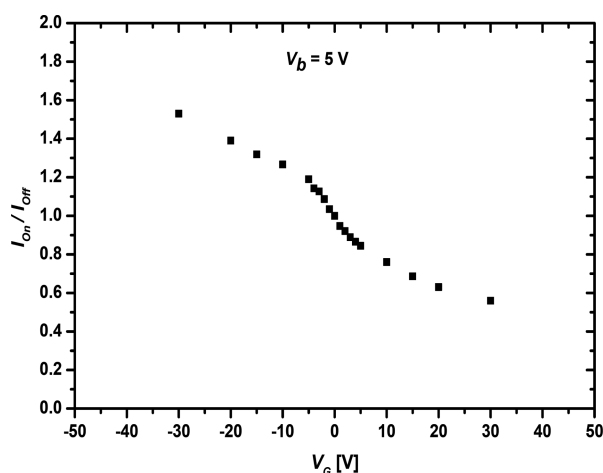
Figure 4. Tunnel current enhancement (I_{On}/I_{Off}) versus gate voltage at 300 K for sample S1. The applied bias voltage is $V_b = 5$ V.

Here, we briefly discuss PNRM, which will enable us to analyze the experimental data obtained from the electrical measurements. According to PNRM, any network of disordered nanoparticles (NPs) can be represented by a network of parallel nonlinear resistors. Each nonlinear resistor is made of one-dimensional (1D) or 2D arrays of NPs. In each nonlinear resistor, NPs have equal Coulomb blockade energies (E_c values) and the tunnel junction gaps (l values) between NPs are equal.[19] The Coulomb blockade energy is the electrostatic energy required to remove one electron from a NP and add to its nearest neighbor.[26] The total tunnel current is then calculated by summing over all these n nonlinear resistors as[19]

$$I = C_1 \sum_i \left\{ \frac{N(E_c^i)}{N_x(E_c^i)} e^{-4\pi \sqrt{2m\left(U - \frac{eV_b}{N_x(E_c^i)}\right)} l(T, E_c^i)/h} \right.$$
$$\left. \left[\frac{E_c^i + \frac{eV_b}{N_x(E_c^i)}}{1 - e^{(E_c^i + \frac{eV_b}{N_x(E_c^i)})/(k_B T)}} - \frac{E_c^i - \frac{eV_b}{N_x(E_c^i)}}{1 - e^{(E_c^i - \frac{eV_b}{N_x(E_c^i)})/(k_B T)}} \right] \right\} \quad (1)$$

where C_1 is a constant related to the tunneling cross-section area and the density of electronic states at the Fermi level of NPs, i labels the nonlinear resistors, N is the total number of

NPs with equal E_c, N_x is the number of tunnel junctions between two contact electrodes in each array (it is assumed $N_x \gg 1$), m is the effective mass of the electron, U is the height of the tunnel barrier, e is the electron charge, T is the absolute temperature, h is the Planck constant, and k_B is the Boltzmann constant.

The precise calculation of E_c values in networks of disordered NPs is extremely difficult because E_c values are affected by surrounding NPs.[19] Therefore, to take into account such an effect, CNTs are represented by coaxial cables, which their Coulomb blockade energies can be calculated as

$$E_c = \frac{e^2 \ln[(2g + d)/d]}{4\pi\varepsilon_0 L} \quad (2)$$

where g is the distance between the surface of the inner conductor (CNT) and the inner surface of the outer conductor (or surrounding CNTs), d is the diameter of the inner conductor (CNT), ε_0 is the permittivity of the free space, and L is the length of the CNT. The number of tunnel junctions, which is a function of E_c, can be estimated as

$$N_x = \frac{L_e}{L} \quad (3)$$

where L_e is the gap between two electrodes. The tunnel junction gap (l) has been neglected in the denominator, as it is on the order of nanometers whereas CNTs can be as long as hundreds of nanometers. CNTs have different diameters and lengths, and one can obtain the same E_c for a CNT by using different values of g, d, and L in eq 2. In addition, the tunnel current can take different values at a fixed value of E_c because N_x is a function of L. Therefore, to obtain the best fit to the experimental data and simplify the calculations, we chose an average value for g and d and only allowed L to take different values to characterize E_c distributions in the samples. The tunnel junction gaps in each 1D array were assumed to be equal, but they will be a function of temperature due to the thermal expansion of tunnel junction gaps.[19,27−29] Here, the following equation is used to obtain the best fit to the experimental data,

$$l(T, E_c^i) = l_0(300 \text{ K})[1 + \gamma(T - 300 \text{ K})] - C_2 E_c^{i\,3/2} \quad (4)$$

where $l_0(300 \text{ K})$ is the tunnel junction gap at 300 K, γ is the thermal expansion coefficient of tunnel junction gaps, and C_2 is a constant. It is important to note that γ is a function of CNT's

Table 1. Parameters Used in Equations 1−4 To Calculate the Tunnel Currents in S1−S5^a

	sample				
	S1	S2	S3	S4	S5
L_{min} [μm]	0.3	0.3	0.3	0.3	0.3
L_{max} [μm]	3	3	3	3	3
E_{cmin} [meV]	1.51	1.51	0.74	0.77	0.79
E_{cmax} [meV]	15.1	15.1	7.4	7.7	7.9
C_1 [($\Omega \cdot C$)$^{-1}$]	7.13×10^{22}	7.13×10^{22}	1.56×10^{24}	2.81×10^{24}	3.25×10^{24}
C_2 [nm/(meV)$^{3/2}$]	8.9×10^{-3}	8.9×10^{-3}	2.15×10^{-2}	1.9×10^{-2}	1.35×10^{-2}
U [eV]	3.5	3.5	3.5	3.5	3.5
l_0(300 K) [nm]	1.31	1.385	1.32	1.31	1.31
γ [K^{-1}]	4.5×10^{-5}	4.5×10^{-5}	5×10^{-5}	5×10^{-5}	5.5×10^{-5}
d [nm]	0.9	0.95	6.5	8.5	9.5
g [nm]	10	10.5	12	17	20
N	1.35×10^6	1×10^6	7×10^5	4×10^5	1.84×10^5
n	1000	1000	1000	1000	1000

^{a}The gap between two electrodes was L_e = 0.2 mm.

diameter (d),[19] which has a different average value in each sample. The E_c distribution in disordered networks such as ours is a random function, which is unknown. Here, for each sample a uniform E_c distribution is considered because there is a broad distribution of E_c values in the networks.

By use of eqs 1−4 and the parameters listed in Table 1, the resistance of samples was calculated at different temperatures at V_b = 1 mV. Figure 5 is a semilogarithmic plot of the normalized
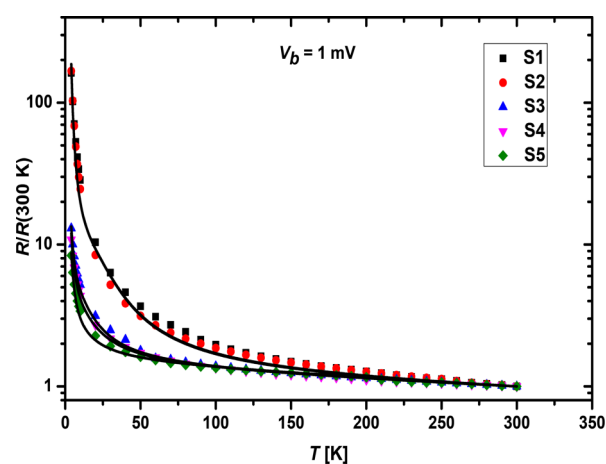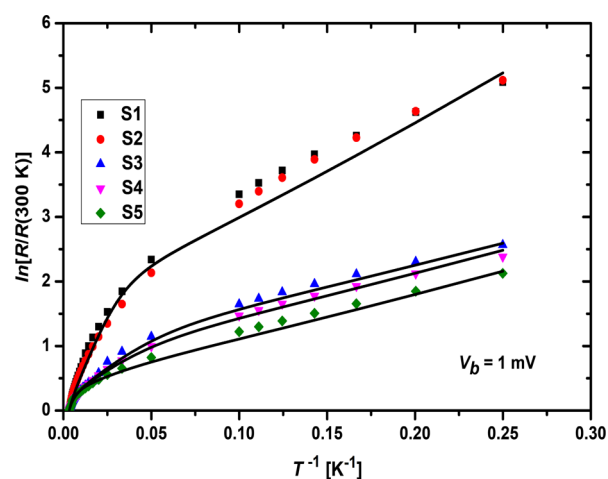

Figure 5. Normalized resistances of S1−S5 as a function of temperature over the temperature range of T = 4−300 K at the bias voltage of V_b = 1 mV. The normalized resistances are plotted in log$_{10}$ scale to better show the experimental data at low temperatures. Solid curves are results of the calculations.

resistances of samples S1−S5 as a function of temperature (4−300 K) at the low bias voltage of V_b = 1 mV. The results of calculations agree very well with the experimental data. The resistance of samples increases exponentially with decreasing temperature, resembling the conduction mechanism in networks of disordered NPs.[19,26−29] By use of eq 3 and L_{max} in Table 1, the maximum electrostatic energy of electrons in S1 at V_b = 1 mV can be estimated as eV_b/N_x = 3/200 meV = 0.015 meV $\ll E_{cmin}$ = 1.51 meV, which means we are in the low voltage regime. At low bias voltages, electrons do not have sufficient electrostatic energy to overcome the Coulomb blockade effect of CNTs and the electron tunneling occurs because of the thermal broadening of the Fermi distribution

(k_BT). The Fermi broadening decreases with temperature, which decreases the tunnel current, and the resistance increases exponentially.[19]

Figure 6 shows that logarithms of normalized resistances change nonlinearly with inverse of temperature (non-Arrhenius


Figure 6. Logarithm of normalized resistances of S1−S5 as a function of inverse of temperature at the bias voltage of V_b = 1 mV. The diagram shows non-Arrhenius behaviors of S1−S5 over the temperature range of T = 4−300 K. Solid curves are results of the calculations.

behavior). The slopes of these diagrams can be related to E_c of CNTs.[19] At low voltage regime and high temperatures ($k_BT \gg E_c$) the slope will be $E_c/3$, and at low temperatures ($k_BT \ll E_c$) the slope will be almost equal to E_c.[19] At high temperatures, a high tunnel current can pass through arrays with the high E_c due to the Fermi broadening; as the temperature decreases, most of the tunnel current will pass through the arrays with the lower E_c because we are at the low voltage regime. Therefore, slopes will decrease with temperature.

To better demonstrate this, the slopes were numerically calculated using eqs 1−4 and the parameters listed in Table 1 at V_b = 1 mV as[19]

$$\text{slope} = \frac{d\ln[R/R(300\text{ K})]}{d(1/T)} \quad (5)$$
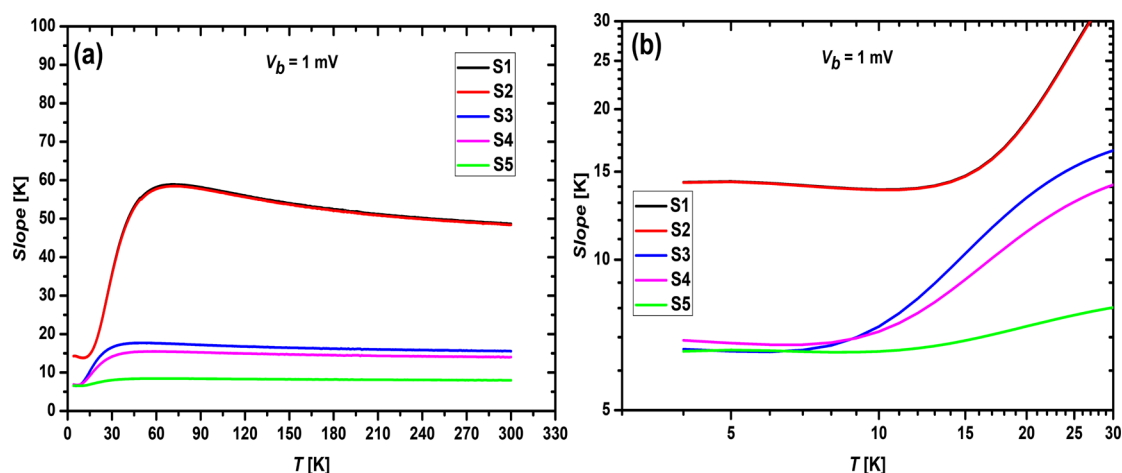
Figure 7. (a) Slopes of diagrams in Figure 6 as a function of temperature at the bias voltage of V_b = 1 mV. (b) Slopes are in $\log_{10}$ scale to better show the data at low temperatures.

Results of the calculations are shown in Figure 7. It can be seen that samples show Arrhenius behavior at high temperatures (constant slopes) and slopes begin to decrease with temperature between two crossover temperature regions. Then, below the second crossover temperature region, slopes become constant again showing Arrhenius behavior. Such behaviors cannot be explained by other theoretical models such as the electron cotunneling model,[21,30] the fluctuation-induced tunneling,[22,23] Efros−Shklovskii and Mott variable range hopping models,[20] as these models only predict the existence of the first crossover temperature. The existence of two crossover temperature regions is only predicted by the percolation model[26] and the PNRM,[19] and they have been experimentally demonstrated in the previous experiments.[19,26]

The recent investigation on networks of s-SWCNTs has shown that the deviation from the Arrhenius behavior at low temperatures is caused by midgap states in s-SWCNTs, which are formed by defects in s-SWCNTs. Therefore, such a behavior was well-described by the fluctuation-induced tunneling model.[23] Although the fluctuation-induced tunneling can occur in S1, this is not the dominant conduction mechanism, as the deviation from the Arrhenius behavior occurs at two crossover temperatures that is caused by the disorder in Coulomb blockade energies.

Assuming an average length for CNTs, from eq 2 one can see that as the diameter of a CNT decreases, the E_c increases meaning that SWCNTs have higher E_c than MWCNTs. Therefore, we would expect the slopes to decrease at high temperatures from S1 to S5 because the amount of SWCNTs decreases from S1 to S4 and vanishes in S5. As a result, the maximum Coulomb blockade energy (E_{cmax}) decreases from S1 to S5 (Table 1). Similarly, the slopes at low temperatures decrease from S1 to S5 as the minimum Coulomb blockade energy (E_{cmin}) decreases from S1 to S5 (Table 1).

Figure 7a shows the slopes decrease with temperature, but from eq 2 it is seen that E_c is not temperature dependent. This behavior is caused by E_c distribution of CNTs (disorder in sizes of CNTs).[19,26] To clarify which conduction mechanism can comprehensively describe the electronic property of the samples, the $I-V_b$ characteristics of samples S1−S5 are plotted in Figure 8.

All of the samples show nonlinear behavior at the lowest temperature (T = 4 K), and they demonstrate ohmic behavior at the highest temperature (T = 300 K). Therefore, Efros−Shklovskii and Mott variable range hopping[20] cannot be used here, as the curvatures of $I-V_b$ plots are temperature dependent. The previous experiments on networks of few-layer graphene sheets[31] and networks of semiconducting PbSe NPs[32] have shown that if TJRs between NPs become higher than the quantum of resistance ($R_Q = h/(2e^2) \approx 12.9$ kΩ), the Coulomb blockade effect will determine the electronic property of the networks. Therefore, the temperature dependency of the curvatures of $I-V_b$ plots can be described as following. At T = 300 K, the Fermi broadening (corresponding to 25.9 meV) becomes comparable to E_{cmax} (15.1 meV) of SWCNTs (Table 1); hence, the tunnel current becomes less sensitive to the bias voltage and ohmic behavior is observed. At T = 4 K, the Fermi broadening (corresponding to 0.345 meV) is negligible compared to E_{cmax}; therefore, the tunnel current becomes very sensitive to the bias voltage and nonohmic behavior is observed (Figure 8).

Although, such $I-V_b$ curves have been explained by the electron cotunneling[21,30] and the fluctuation-induced tunneling[22] models, they did not predict the observed behaviors at low bias voltages (Figure 7). Therefore, from our model calculations it becomes evident that the PNRM can fully describe the electronic property of S1−S5 over a wide temperature range (4−300 K) at broad bias voltages (0.001−10 V).

It is important to note that the purity and concentration of s-SWCNTs and the channel length in FETs made of networks of s-SWCNTs can significantly affect the efficiency of FETs (I_{On}/I_{Off}). These investigations have shown that metallic SWCNTs as impurities can dramatically decrease I_{On}/I_{Off} in networks of s-SWCNT FETs.[33,34] On the one hand, I_{On}/I_{Off} decreases with increasing the density of s-SWCNTs. On the other hand, I_{On}/I_{Off} increases with decreasing the channel length.[34]

Even though the role of metallic SWCNTs in the electron transport mechanism of networks of s-SWCNTs has been considered,[33,34] the Coulomb blockade effect of SWCNTs has not been investigated. The recovery of semiconducting property of individual s-SWCNTs in dense networks of purified s-SWCNTs indicates that the TJRs between s-SWCNTs have been smaller than the quantum of resistance (R_Q). Therefore, the Coulomb blockade effect of s-SWCNTs did not affect the semiconducting property of the networks. Unlike the previous
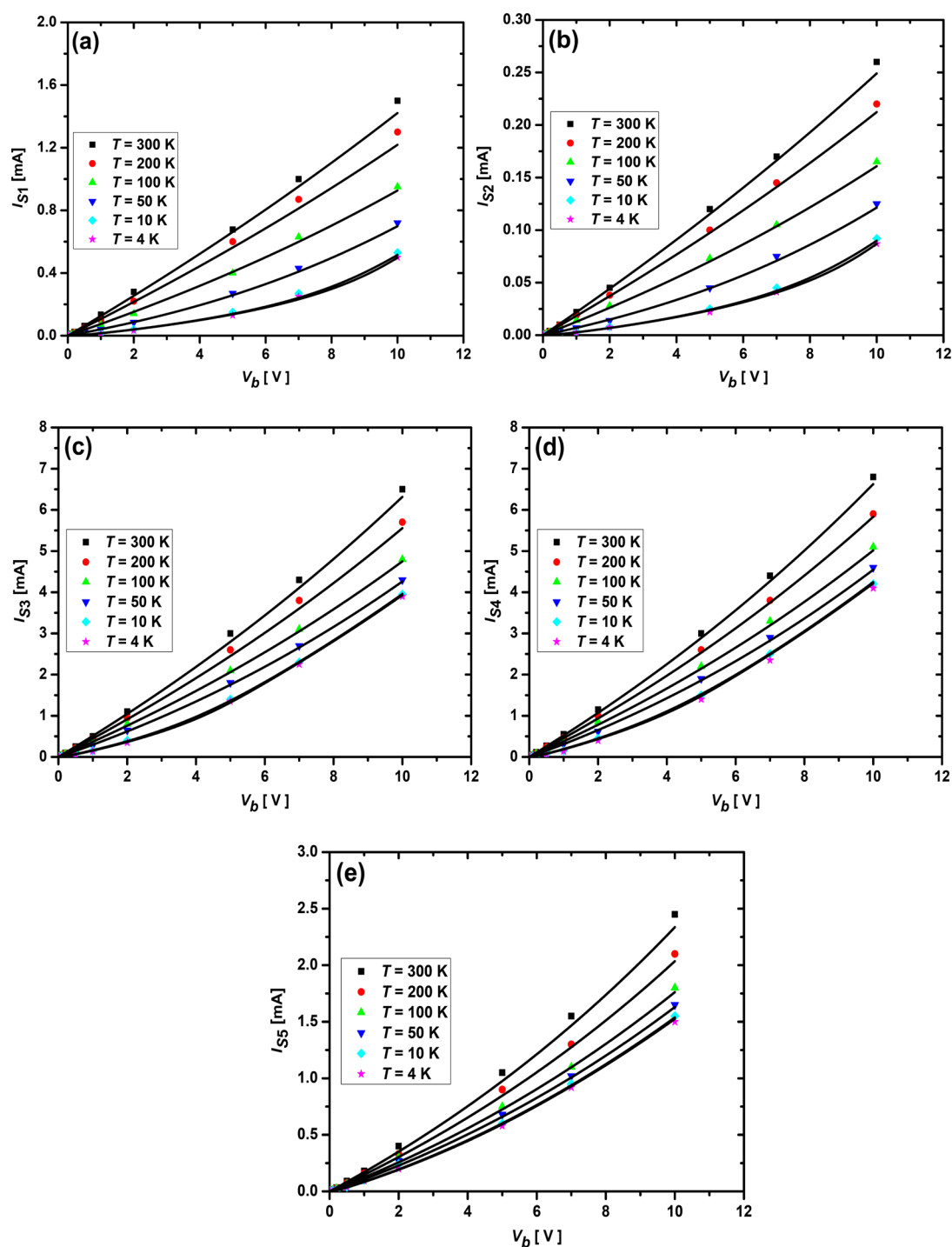
Figure 8. (a) Tunnel current versus bias voltage ($I-V_b$) of S1, (b) S2, (c) S3, (d) S4, and (e) S5 at six different temperatures. In all of the samples, nonlinearity of the curves increases as the temperature decreases.

experiments,[33,34] we did not observe any tunnel current saturation at negative bias voltages. In addition, Raman spectroscopy (RBM modes) indicated that the concentration of metallic SWCNTs in S1 is not very high. Most importantly, the conduction mechanism in sample S1 was quite similar to samples S2−S5 which had much higher concentration of metallic CNTs and our model calculations agreed very well with the experimental data over a wide temperature range (4−300 K) at broad bias voltages (0.001−10 V) indicating that the Coulomb blockade effect of metallic SWCNTs in samples S1−S4 was dominant compared to the metallic property of

SWCNTs. Furthermore, if the TJRs between metallic CNTs in samples S1−S5 were less than R_Q, then their metallic property would be observed as reported in previous experiments on networks of gold nanoislands.[27] Therefore, the low efficiency of FET made of networks of SWCNTs in S1 is mainly caused by the tunnel junctions between SWCNTs and the Coulomb blockade effect of SWCNTs.

■ **CONCLUSIONS**

This investigation revealed that if TJRs in networks of s-SWCNTs become higher than the quantum of resistance (R_Q),

the overlap of electron wave functions between s-SWCNTs becomes negligible and the electrons are strongly localized within s-SWCNTs. As a result, TJRs in networks of s-SWCNTs do not significantly affect the optical property of individual s-SWCNTs and such networks can be used in applications that only require optical measurements. Our model calculations based on the PNRM[19] showed the observed transition from Arrhenius to non-Arrhenius behavior that occurred at two different temperature regions, and the temperature-dependent curvature of the current−voltage characteristics of the networks is caused by disorder in the Coulomb blockade energies of CNTs. Furthermore, in networks of s-SWCNTs the Coulomb blockade effect dominates the electronic property of the networks, which significantly decreases the efficiency of FETs made of s-SWCNT networks. To overcome this shortcoming, one can use a high density of purified s-SWCNTs where TJRs become smaller than the quantum of resistance.

■ AUTHOR INFORMATION

Notes
The authors declare no competing financial interest.

■ ACKNOWLEDGMENTS

■ REFERENCES

(1) Javey, A.; Guo, J.; Wang, Q.; Lundstrom, M.; Dai, H. Ballistic Carbon Nanotube Field-Effect Transistors. *Nature* **2003**, *424*, 654−657.

(2) Franklin, A. D.; Chen, Z. Length Scaling of Carbon Nanotube Transistors. *Nat. Nanotechnol.* **2010**, *5*, 858−862.

(3) Tans, S. J.; Verschueren, A. R. M.; Dekker, C. Room-Temperature Transistor Based on a Single Carbon Nanotube. *Nature* **1998**, *393*, 49−52.

(4) Alhassen, H.; Antony, V.; Ghanem, A.; Yajadda, M. M. A.; Han, Z. J.; Ostrikov, K. K. Organic/Hybrid Nanoparticles and Single-Walled Carbon Nanotubes: Preparation Methods and Chiral Applications. *Chirality* **2014**, *26*, 683−691.

(5) Ahmed, M.; Yajadda, M. M. A.; Han, Z. J.; Su, D.; Wang, G.; Ostrikov, K. K.; Ghanem, A. Single-Walled Carbon Nanotube-Based Polymer Monoliths for the Enantioselective Nano-liquid Chromatographic Separation of Racemic Pharmaceuticals. *J. Chromatogra. A* **2014**, *1360*, 100−109.

(6) Yick, S.; Yajadda, M. M. A.; Bendavid, A.; Han, Z. J.; Ostrikov, K. K. Physisorption-Induced Electron Scattering on the Surface of Carbon-Metal Core-Shell Nanowire Arrays for Hydrogen Sensing. *Appl. Phys. Lett.* **2013**, *102*, 233111−233114.

(7) Ghosh, S.; Sood, A. K.; Kumar, N. Carbon Nanotube Flow Sensors. *Science* **2003**, *299*, 1042−1044.

(8) Snow, E. S.; Perkins, F. K.; Houser, E. J.; Badescu, S. C.; Reinecke, T. L. Chemical Detection with a Single-Walled Carbon Nanotube Capacitor. *Science* **2005**, *307*, 1942−1945.

(9) Barone, P. W.; Baik, S.; Heller, D. A.; Strano, M. S. Near-Infrared Optical Sensors Based on Single-Walled Carbon Nanotubes. *Nat. Mater.* **2005**, *4*, 86−92.

(10) Wang, J. Carbon-Nanotube Based Electrochemical Biosensors: A Review. *Electroanalysis* **2005**, *17*, 7−14.

(11) Salehi-Khojin, A.; Khalili-Araghi, F.; Kuroda, M. A.; Lin, K. Y.; Leburton, J. P.; Masel, R. I. On the Sensing Mechanism in Carbon Nanotube Chemiresistors. *ACS Nano* **2011**, *5*, 153−158.

(12) Nirmalraj, P. N.; Lyons, P. E.; De, S.; Coleman, J. N.; Boland, J. J. Electrical Connectivity in Single-Walled Carbon Nanotube Networks. *Nano Lett.* **2009**, *9*, 3890−3895.

(13) Yanagi, K.; Udoguchi, H.; Sagitani, S.; Oshima, Y.; Takenobu, T.; Kataura, H.; Ishida, T.; Matsuda, K.; Maniwa, Y. Transport Mechanisms in Metallic and Semiconducting Single-Wall Carbon Nanotube Networks. *ACS Nano* **2010**, *4*, 4027−4032.

(14) Bekyarova, E.; Itkis, M. E.; Cabrera, N.; Zhao, B.; Yu, A.; Gao, J.; Haddon, R. C. Electronic Properties of Single-Walled Carbon Nanotube Networks. *J. Am. Chem. Soc.* **2005**, *127*, 5990−5995.

(15) Yosida, Y.; Oguro, I. Variable Range Hopping Conduction in Bulk Samples Composed of Single-Walled Carbon Nanotubes. *J. Appl. Phys.* **1999**, *86*, 999−1003.

(16) Blackburn, J. L.; Barnes, T. M.; Beard, M. C.; Kim, Y. H.; Tenent, R. C.; McDonald, T. J.; To, B.; Coutts, T. J.; Heben, M. J. Transparent Conductive Single-Walled Carbon Nanotube Networks with Precisely Tunable Ratios of Semiconducting and Metallic Nanotubes. *ACS Nano* **2008**, *2*, 1266−1274.

(17) Han, Z. J.; Yick, S.; Levchenko, I.; Tam, E.; Yajadda, M. M. A.; Kumar, S.; Martin, P. J.; Furman, S.; Ostrikov, K. K. Controlled Synthesis of a Large Fraction of Metallic Single-Walled Carbon Nanotube and Semiconducting Carbon Nanowire Networks. *Nanoscale* **2011**, *3*, 3214−3220.

(18) Fuhrer, M. S.; Cohen, M. L.; Zettl, A.; Crespi, V. Localization in Single-Walled Carbon Nanotubes. *Solid State Commun.* **1998**, *109*, 105−109.

(19) Yajadda, M. M. A. Calculating Electronic Tunnel Currents in Networks of Disordered Irregularly Shaped Nanoparticles by Mapping Networks to Arrays of Parallel Nonlinear Resistors. *J. Appl. Phys.* **2014**, *116*, 153707−153719.

(20) Shklovskii, B. I.; Efros, A. L. *Electronic Properties of Doped Semiconductors*; Springer-Verlag: New York, 1984.

(21) Tran, T. B.; Beloborodov, I. S.; Hu, J.; Lin, X. M.; Rosenbaum, T. F.; Jaeger, H. M. Sequential Tunneling and Inelastic Cotunneling in Nanoparticle Arrays. *Phys. Rev. B: Condens. Matter Mater. Phys.* **2008**, *78*, 075437.

(22) Sheng, P. Fluctuation-Induced Tunneling Conduction in Disordered Materials. *Phys. Rev. B: Condens. Matter Mater. Phys.* **1980**, *21*, 2180−2195.

(23) Itkis, M. E.; Pekker, A.; Tian, X.; Bekyarova, E.; Haddon, R. C. Networks of Semiconducting SWNTs: Contribution of Midgap Electronic States to the Electrical Transport. *Acc. Chem. Res.* **2015**, *48*, 2270−2279.

(24) Liu, H.; Nishide, D.; Tanaka, T.; Kataura, H. Large-Scale Single-Chirality Separation of Single-Wall Carbon Nanotubes by Simple Gel Chromatography. *Nat. Commun.* **2011**, *2*, 309−316.

(25) Yan, L. Y.; Li, W.; Mesgari, S.; Leong, S. S. J.; Chen, Y.; Loo, L. S.; Mu, Y.; Chan-Park, M. B. Use of a Chondroitin Sulfate Isomer as an Effective and Removable Dispersant of Single-Walled Carbon Nanotubes. *Small* **2011**, *7* (19), 2758−2768.

(26) Müller, K.-H.; Yajadda, M. M. A. Electron Transport in Discontinuous Gold Films and the Effect of Coulomb Blockade and Percolation. *J. Appl. Phys.* **2012**, *111*, 123705−123715.

(27) Yajadda, M. M. A.; Müller, K.-H.; Ostrikov, K. K. Effect of Coulomb Blockade, Gold Resistance, and Thermal Expansion on the Electrical Resistance of Ultrathin Gold Films. *Phys. Rev. B: Condens. Matter Mater. Phys.* **2011**, *84*, 235431−235438.

(28) Byeon, J. H.; Roberts, J. T. Aerosol Based Fabrication of Thiol-Capped Gold Nanoparticles and Their Application for Gene Transfection. *Chem. Mater.* **2012**, *24*, 3544−3549.

(29) Moreira, H.; Grisolia, J.; Sangeetha, N. M.; Decorde, N.; Farcau, C.; Viallet, B.; Chen, K.; Viau, G.; Ressier, L. Electron Transport in Gold Colloidal Nanoparticle-Based Strain Gauges. *Nanotechnology* **2013**, *24*, 095701−095709.

(30) Dugay, J.; Tan, R. P.; Ibrahim, M.; Garcia, C.; Carrey, J.; Lacroix, L.-M.; Fazzini, P.-F.; Viau, G.; Respaud, M. Charge Transport and Interdot Coupling Tuned by the Tunnel Barrier Length in Assemblies of Nanoparticles Surrounded by Organic Ligands. *Phys. Rev. B: Condens. Matter Mater. Phys.* **2014**, *89*, 041406(R).

(31) Yajadda, M. M. A.; Kumar, S.; Ostrikov, K. K. The Role of Tunnel Junction Resistances and Defects on Electron Transport

Mechanism in Networks of Two-Dimensional Disordered Conductors. *Phys. E* **2014**, *64*, 87−94.

(32) Romero, H. E.; Drndic, M. Coulomb Blockade and Hopping Conduction in PbSe Quantum Dots. *Phys. Rev. Lett.* **2005**, *95*, 156801.

(33) Wang, C.; Zhang, J.; Ryu, K.; Badmaev, A.; De Arco, L. G.; Zhou, C. Wafer-Scale Fabrication of Separated Carbon Nanotube Thin-Film Transistors for Display Applications. *Nano Lett.* **2009**, *9*, 4285−4291.

(34) Rouhi, N.; Jain, D.; Zand, K.; Burke, P. J. Fundamental Limits on the Mobility of Nanotube-Based Semiconducting Inks. *Adv. Mater.* **2011**, *23*, 94−99.